

Observational constraints on non-flat dynamical dark energy cosmological models

Omer Farooq,^{a,1} Data Mania,^{a,b} Bharat Ratra^a

^aDepartment of Physics, Kansas State University, 116 Cardwell Hall, Manhattan 66506 USA

^bCenter for Elementary Particle Physics, Ilia State University, 3-5 Cholokashvili Ave., Tbilisi 0179, Georgia

E-mail: omer@phys.ksu.edu, mania@phys.ksu.edu, ratra@phys.ksu.edu

Abstract.

We constrain two non-flat time-evolving dark energy cosmological models by using Hubble parameter data, Type Ia supernova apparent magnitude measurements, and baryonic acoustic oscillation peak length scale observations. The inclusion of space curvature as a free parameter in the analysis results in a significant broadening of the allowed range of values of the parameter that governs the time evolution of the dark energy density in these models. While consistent with the “standard” spatially-flat Λ CDM cosmological model, these data are also consistent with a range of mildly non-flat, slowly time-varying dark energy models. After marginalizing over all other parameters, these data require the averaged magnitude of the curvature density parameter $|\Omega_{k0}| \lesssim 0.15$ at 1σ confidence.

¹Corresponding author.

Contents

1	Introduction	1
2	Time-varying dark energy models in curved space	3
3	Observational constraints	6
3.1	Constraints from $H(z)$, SNIa, and BAO data sets, one at a time	6
3.2	Constraints from combinations of data sets	10
4	Conclusion	12

1 Introduction

There is significant observational evidence that the Universe is currently undergoing accelerated expansion. Most cosmologists believe that dark energy dominates the current cosmological energy budget and is responsible for this accelerated expansion [for reviews of dark energy see 61, 93, 102, and references therein].⁴ In addition, if one assumes that the dark energy density is close to or time independent, cosmic microwave background (CMB) anisotropy measurements indicate that the Universe must be close to or spatially flat (Ade et al. 1 and references therein; for an early indication see Podariu et al. 80). Conversely, if one assumes that the space sections are flat, the data favor a time-independent cosmological constant. However, as far as we are aware, there has not been an analysis of observational data based on a physically consistent non-spatially-flat dynamical dark energy model. In this paper we present the first such analysis.

As a warm-up exercise, we consider the popular Λ CDM parameterization of dynamical dark energy.⁵ We generalize this parameterization to the case when the spatial hypersurfaces have non-zero curvature, a case that has been considered previously, along with more general fluid parameterizations [see e.g., 31, 35, 46, 52–55, 68, 103, 107, 113]. These authors [also see 110] emphasize the important point that in this case there is a degeneracy between the spatial curvature and the X -fluid equation of state parameter, and so cosmological data are not as constraining in this case compared to the case when either spatial curvature vanishes or the dark energy density is a constant. However, the Λ CDM parameterization is incomplete, as it does not describe spatial inhomogeneities [see e.g., 81, 82].

The Λ CDM parameterization is a generalization of the standard Λ CDM cosmological model [73]. In the Λ CDM case the current energy budget is dominated by a time-independent cosmological constant Λ . It is well-known that the Λ CDM model has some puzzling features

⁴ Some instead argue that these observations should be viewed as an indication that general relativity needs to be modified on these large cosmological length scales. For recent reviews of modified gravity see [22], [101], and references therein. We assume here that general relativity provide an accurate description of gravitation on cosmological length scales.

⁵Here dark energy is taken to be a spatially-homogeneous X -fluid with a time-evolving energy density that dominates the current cosmological energy budget, with non-relativistic cold dark matter (CDM) being the next largest contributor.

which are more easily understood if, instead of remaining constant like Λ , the dark energy density gradually decreases with time.⁶

The simplest, complete and consistent time-varying dark energy model is ϕ CDM [74, 84].⁷ Here dark energy is modeled as a scalar field, ϕ , with a gradually decreasing (in ϕ) potential energy density $V(\phi)$. In this paper we assume an inverse-power-law potential energy density, $V(\phi) \propto \phi^{-\alpha}$, where α is a nonnegative constant [74]. At $\alpha = 0$ the ϕ CDM model reduces to the corresponding Λ CDM case. The ϕ CDM model was originally formulated in a spatially-flat cosmological model. In this paper we consider the [72] generalization of the ϕ CDM model to non-flat space.⁸

For some time now, most observational constraints have been reasonably consistent with the predictions of the “standard” spatially-flat Λ CDM model [for early indications see e.g., 2, 32, 56, 109]. The big four, CMB anisotropy [e.g., 1], supernova Type Ia (SNIa) apparent magnitude versus redshift [e.g., 21, 87, 97], baryonic acoustic oscillation (BAO) peak length scale [e.g., 13, 15, 66, 76], and Hubble parameter as a function of redshift [e.g., 18, 27, 39, 67] measurements provide the strongest support for this conclusion.

Other measurements that have been used to constrain cosmological parameters include, for example, galaxy cluster gas mass fraction as a function of redshift [e.g., 2, 58, 63, 88, 100], galaxy cluster and other large-scale structure properties [10, 33, 34, 69, 106, and references therein], gamma-ray burst luminosity distance as a function of redshift [e.g., 19, 70, 89, 104], HII starburst galaxy apparent magnitude as a function of redshift [e.g., 65, 77, 78], angular size as a function of redshift [e.g., 16, 28, 50], and strong gravitational lensing [14, 23, 59, 96, and references therein].⁹ While the constraints from these data are typically less restrictive than those derived from the $H(z)$, SNIa, CMB anisotropy, and BAO data, both types of measurements result in largely compatible constraints that generally support a currently accelerating cosmological expansion. This provides confidence that the broad outlines of a “standard” cosmological model are now in place.

In this paper we consider an extension of this “standard” cosmological model by allowing for the possibility of non-zero space curvature. As mentioned above, we consider two possibilities, a generalization of the Λ CDM parameterization as well as the [72] generalization of the ϕ CDM model. In this paper we derive constraints on the parameters of these options by using $H(z)$, SNIa, and BAO data. This work extends previous work [e.g. 37–39] via the inclusion of space curvature in dynamical dark energy models.

Here we do not make use of the last of the big four data, that of CMB anisotropy. While CMB anisotropy data are widely credited with providing the strongest evidence for a very small contribution to the current energy budget from spatial curvature (however, see discussion above), it is not straightforward to include them because they require an analysis of the evolution of spatial inhomogeneities. In the case of the Λ CDM parametrization this

⁶Note that there also are tentative observational indications that the standard CDM structure formation model, which is assumed in the Λ CDM cosmological model, might need to be improved upon [75, 108, and references therein].

⁷For recent discussions of other time-varying dark energy models see [62], [44], [11], [8], [40], [12], [60], and references therein.

⁸Curved-space scalar field dark energy models have been studied in the past [see e.g., 5–7, 29, 51, 99]. However, as far as we are aware, [72] were the first to establish that the scalar field solution is a time-dependent fixed point or attractor even in the curvature dominated epoch.

⁹Future space-based SNIa and BAO-like measurements [e.g., 9, 71, 79, 90, 91], as well as measurements based on new techniques [3, 4, and references therein] should soon provide interesting constraints on cosmological parameters.

is not possible without an ad hoc extension. In the ϕ CDM case this requires a detailed computation, including the assumption of an early epoch of inflation in non-flat space and a derivation of the concomitant power spectrum needed for the CMB anisotropy computation. It is well known that the observed CMB anisotropy is almost certainly a consequence of quantum-mechanical zero-point fluctuations generated during inflation [see e.g., 41, 83]. While conceptually similar, the computation of the primordial spectrum is more involved in the spatially-curved case than in the flat model [see e.g., 17, 43, 47, 48, 57, 64, 85, 86, 111]. Consequently, the computation of CMB anisotropy constraints is beyond the scope of this initial paper. Even though we do not use CMB anisotropy constraints here, a combination of the other three of the big four data— $H(z)$, SNIa, and BAO— results in reasonably tight constraints on space curvature. For technical computational reasons we believe our XCDM parametrization constraints are more reflective of the true constraints on space curvature.¹⁰ In the XCDM case, marginalizing over all other parameters, the $H(z)$, SNIa, and BAO data require $|\Omega_{k0}| \leq 0.15$ and 0.3 at about 1σ and 2σ confidence.

Our paper is organized as follows. In Sec. 2 we present the basic equations of the ϕ CDM dark energy model and the XCDM dark energy parameterization. Constraints from observational data are derived in Sec. 3. We conclude in Sec. 4.

2 Time-varying dark energy models in curved space

In this section we summarize the two models we constrain. These are the [72] generalization to curved space of the time-evolving dark energy ϕ CDM model [74, 84], as well as the curved space generalization of the widely-used XCDM dynamic dark energy parameterization in which dark energy is modeled as a spatially-homogeneous time-dependent X -fluid.

We assume that general relativity provides an accurate description of gravitation on cosmological scales. The equations of motion are Einstein’s field equations,

$$R_{\mu\nu} - \frac{1}{2}Rg_{\mu\nu} = 8\pi GT_{\mu\nu} - \Lambda g_{\mu\nu}. \quad (2.1)$$

Here $R_{\mu\nu}$ and R are the Ricci tensor and scalar, $g_{\mu\nu}$ is the metric tensor, Λ is the cosmological constant, $T_{\mu\nu}$ is the energy-momentum tensor of the matter present, and G is the Newtonian gravitational constant.

At late times we can ignore radiation and model non-relativistic (cold dark and baryonic) matter as a perfect fluid with energy-momentum tensor $T_{\mu\nu} = \text{diag}(\rho, p, p, p)$ where ρ and p are the energy density and the pressure of the fluid. Assuming the cosmological principle of spatial homogeneity, Einstein’s equations reduce to the two independent Friedmann equations,

$$\left(\frac{\dot{a}}{a}\right)^2 = \frac{8\pi G}{3}\rho - \frac{K^2}{a^2} + \frac{\Lambda}{3}, \quad (2.2)$$

$$\frac{\ddot{a}}{a} = -\frac{4\pi G}{3}(\rho + 3p) + \frac{\Lambda}{3}. \quad (2.3)$$

Here $a(t)$ is the cosmological scale factor, which is the ratio of the physical distance to the moving distance of a sufficiently distant object (so that the spatial homogeneity assumption is valid), an over-dot denotes a derivative with respect to cosmological time, K^2 represents

¹⁰It is much more time consuming to do the ϕ CDM computation, so we assumed a narrower prior on space curvature in this case, which we suspect leads to slightly tighter but less reliable constraints.

the curvature of spatial hypersurfaces (and can have three discrete values -1 , 0 , or $+1$, corresponding to hyperbolic, flat, and spherical geometry respectively), and ρ and p are the sums of all (time-dependent) densities and pressures of the various forms of matter present.

With a single type of matter, the Friedmann equations (2.2)—(2.3) are two equations with three time-dependent unknowns, $a(t)$, $\rho(t)$, and $p(t)$. We can complete the system of equations with an equation of state for each type of matter. This is a relation between pressure and energy density for each type of matter,

$$p = p(\rho) = \omega\rho, \quad (2.4)$$

where ω is the dimensionless equation-of-state parameter for an ideal fluid. For non-relativistic matter $\omega = 0$, while $\omega = -1$ corresponds to a standard cosmological constant Λ , and $\omega < -1/3$ corresponds to the Λ CDM parameterization.

Equations (2.2)—(2.4) form a closed set and can be used to derive the energy conservation equation,

$$\frac{\dot{\rho}}{\rho} = -3 \frac{\dot{a}}{a} (1 + \omega). \quad (2.5)$$

This first-order linear differential equation can be solved with the boundary condition $\rho(t_0) = \rho_0$, where t_0 is the current time and ρ_0 is the current value of the energy density of the particular type of matter under consideration. The solution is

$$\rho(t) = \rho_0 \left(\frac{a_0}{a} \right)^{3(1+\omega)}, \quad (2.6)$$

where a_0 is the current value of the scale factor. If there are a number of different species of non-interacting fluids, then Eq. (2.6) holds separately for each of them with the corresponding ω and ρ_0 . For a non-relativistic gas (cold matter) $\omega = \omega_m = 0$ and $\rho_m \propto a^{-3}$, for a homogeneous X -fluid $\omega = \omega_X < -1/3$ and $\rho_X \propto a^{-3(1+\omega_X)}$, and for spatial curvature $\omega = \omega_K = -1/3$ and $\rho_K \propto a^{-2}$.

The ratio $\dot{a}(t)/a(t)$ in Eq. (2.2) is the Hubble parameter $H(t)$. The present value of the Hubble parameter is the Hubble constant H_0 . To rewrite the Friedmann equation (2.2) in terms of observable parameters we define the dimensionless redshift $z = a_0/a - 1$, and the present value of the density parameters,

$$\Omega_{m0} = \frac{8\pi G\rho_{m0}}{3H_0^2}, \quad \Omega_{K0} = \frac{-K^2}{(H_0 a_0)^2}, \quad \Omega_{X0} = \frac{8\pi G\rho_{X0}}{3H_0^2}. \quad (2.7)$$

Here we have parameterized dark energy as a spatially homogeneous X -fluid with current density parameter value Ω_{X0} , Ω_{m0} is the current non-relativistic (baryonic and cold dark) matter density parameter, and Ω_{K0} is that of spatial curvature (with $\Omega_{K0} > 0$ corresponding to an open or hyperbolic spatial geometry). With these definitions Eq. (2.2) becomes

$$H^2(z; H_0, \mathbf{p}) = H_0^2 \left[\Omega_{m0}(1+z)^3 + (1 - \Omega_{m0} - \Omega_{K0})(1+z)^{3(1+\omega_X)} + \Omega_{K0}(1+z)^2 \right], \quad (2.8)$$

where we have made use of $\Omega_{X0} = 1 - \Omega_{m0} - \Omega_{K0}$. This is the Friedmann equation for the Λ CDM parameterization with non-zero spatial curvature. In this case the cosmological parameters are taken to be $\mathbf{p} = (\Omega_{m0}, \omega_X, \Omega_{K0})$. The Λ CDM parameterization is incomplete, as it cannot describe the evolution of energy density inhomogeneities [see e.g., 81, 82].

The second model we consider is the simplest, complete and consistent dynamical dark energy model, ϕ CDM, generalized to include non-zero spatial curvature [72]. In this case

dark energy is modeled as a slowly-rolling scalar field ϕ with an, e.g., inverse-power-law potential energy density $V(\phi) = \kappa m_p^2 \phi^{-\alpha}/2$ where $m_p = 1/\sqrt{G}$ is the Planck mass and α is a non-negative parameter that determines the coefficient κ [74]. The scalar field part of the ϕ CDM model action is

$$S = \frac{m_p^2}{32\pi} \int \sqrt{-g} (g^{\mu\nu} \partial_\mu \phi \partial_\nu \phi - \kappa m_p^2 \phi^{-\alpha}) d^4x, \quad (2.9)$$

where the parameter κ is [72, 74]

$$\kappa = \frac{8}{3} \left(\frac{2\alpha}{3}\right)^{\alpha/2} (\alpha + 4)(\alpha + 2)^{(\alpha-2)/2}. \quad (2.10)$$

In this model, at the current epoch, scalar field dark energy dominates the cosmological energy budget and fuels the accelerating cosmological expansion. Prior to that space curvature dominated and at even earlier times non-relativistic matter powered the decelerating cosmological expansion. In the matter dominated epoch at $a \ll a_0$, $\rho_\phi \ll \rho_m$ and $\rho_K \ll \rho_m$, the Einstein-de Sitter model applies, and the initial conditions are that the cosmological scale factor evolves as $a(t) \propto t^{2/3}$, the scalar field $\phi(t) \propto t^{2/(\alpha+2)}$, and the scalar field energy density evolves as $\rho_\phi \propto a^{-3\alpha/(\alpha+2)} \propto t^{-2\alpha/(\alpha+2)}$, as described in [74]. In the space curvature dominated epoch $\rho_\phi \ll \rho_K$ and $\rho_m \ll \rho_K$ and $a(t) \propto t$, the scalar field $\phi(t) \propto t^{2/(2+\alpha)}$, and the scalar field energy density evolves as $\rho_\phi \propto a^{-2\alpha/(2+\alpha)} \propto t^{-2\alpha/(2+\alpha)}$,¹¹ as determined in [72]. Hence, for positive values of α , the scalar field energy decreases, but less rapidly than that of space curvature in the space curvature dominated epoch ($\rho_K \propto a^{-2} \propto t^{-2}$) and less rapidly than that of non-relativistic matter in the matter dominated epoch ($\rho_m \propto a^{-3} \propto t^{-2}$), so at late times the Universe will become dark energy dominated [72, 84]. As in the radiation and matter dominated epochs [74, 84], [72] show that in the curvature dominated epoch the solution for the scalar field is a time-dependent fixed point or attractor. This means that for a wide range of initial conditions the solution will approach this special time-dependent fixed point solution.

The equation of motion of the scalar field is,

$$\ddot{\phi} + 3\frac{\dot{a}}{a}\dot{\phi} - \frac{\kappa}{2}\alpha m_p^2 \phi^{-(\alpha+1)} = 0. \quad (2.11)$$

In the presence of spatial curvature the ϕ CDM model Friedmann equation takes the form

$$H^2(z; H_0, \mathbf{p}) = H_0^2 [\Omega_{m0}(1+z)^3 + \Omega_\phi(z, \alpha) + \Omega_{K0}(1+z)^2], \quad (2.12)$$

where the time-dependent scalar field density parameter Ω_ϕ is defined as

$$\Omega_\phi(z, \alpha) \equiv \frac{8\pi G}{3H_0^2} \rho_\phi = \frac{1}{12H_0^2} (\dot{\phi}^2 + \kappa m_p^2 \phi^{-\alpha}). \quad (2.13)$$

In the limit $\alpha = 0$ the ϕ CDM model is equivalent to the ordinary time-independent cosmological constant Λ model. This makes the ϕ CDM model a generalization of the standard Λ CDM model of cosmology.

Solving the coupled differential equations (2.11)–(2.13), with the initial conditions described in [74] and [72], allows for a numerical computation of the Hubble parameter $H(z; H_0, \mathbf{p})$, as well as the other functions needed for applications of the cosmological tests. In this case the model parameters are taken to be $\mathbf{p} = (\Omega_{m0}, \alpha, \Omega_{K0})$.

¹¹As long as the scalar field energy density does not dominate, the scalar field energy density $\rho_\phi \propto t^{-2\alpha/(2+\alpha)}$, independent of the type of matter that dominates.

3 Observational constraints

To constrain cosmological parameters \mathbf{p} we generalize the technique described in [38] to models with three free parameters, $\mathbf{p} = (\Omega_{m0}, \omega_X, \Omega_{K0})$ for the XCDM parameterization and $\mathbf{p} = (\Omega_{m0}, \alpha, \Omega_{K0})$ for ϕ CDM. Following [37] we compute a likelihood function $\mathcal{L}(\mathbf{p})$ that depends on the three \mathbf{p} parameters. We compute these likelihood functions over the parameter ranges $-0.7 \leq \Omega_{K0} \leq 0.7$, $-2.0 \leq \omega_X \leq 0$, and $0 \leq \Omega_{m0} \leq 1.0$ for the XCDM parameterization, and $-0.2 \leq \Omega_{K0} \leq 0.2$, $0 \leq \alpha \leq 5$, and $0 \leq \Omega_{m0} \leq 1.0$ for the ϕ CDM model. For the sake of computational tractability the Ω_{K0} range considered in the case of ϕ CDM is much smaller than that used in the XCDM parameterization computation.

To get two-dimensional likelihood functions $\mathcal{L}(\boldsymbol{\theta})$, we marginalize the three-dimensional likelihood function $\mathcal{L}(\mathbf{p})$ over each of the three model parameters in turn, with flat priors. Here

$$\mathcal{L}(\boldsymbol{\theta}) \equiv \int_{\beta_1}^{\beta_2} \mathcal{L}(\mathbf{p}) d\beta = \int_{\beta_1}^{\beta_2} \mathcal{L}(\boldsymbol{\theta}, \beta) d\beta, \quad (3.1)$$

where $\boldsymbol{\theta}$ is the set of two parameters at a time and β is the third parameter with marginalization limits of β_1 and β_2 .

To maximize the two-dimensional likelihood function $\mathcal{L}(\boldsymbol{\theta})$ we minimize $\chi^2(\boldsymbol{\theta}) \equiv -2\ln\mathcal{L}(\boldsymbol{\theta})$ with respect to model parameters $\boldsymbol{\theta}$ to find the best-fit parameter values $\boldsymbol{\theta}_0$. We define 1σ , 2σ , and 3σ confidence contours as two-dimensional parameter sets bounded by $\chi^2(\boldsymbol{\theta}) = \chi^2(\boldsymbol{\theta}_0) + 2.3$, $\chi^2(\boldsymbol{\theta}) = \chi^2(\boldsymbol{\theta}_0) + 6.17$, and $\chi^2(\boldsymbol{\theta}) = \chi^2(\boldsymbol{\theta}_0) + 11.8$, respectively.¹²

3.1 Constraints from $H(z)$, SNIa, and BAO data sets, one at a time

We first consider $H(z)$ data constraints. For this we use 22 independent $H(z)$ measurements and one standard deviation uncertainties at measured redshifts (covering the redshift range of 0.09 to 2.3), listed in Table 1,¹³ to constrain cosmological model parameters \mathbf{p} . Using Eq. (18) of [37], which is obtained after marginalizing over the nuisance parameter H_0 using a Gaussian prior with $H_0 = 68 \pm 2.8 \text{ km s}^{-1} \text{ Mpc}^{-1}$,¹⁴ we get a likelihood function $\mathcal{L}_H(\mathbf{p})$ that depends only on model parameters $\mathbf{p} = (\Omega_{m0}, \omega_X, \Omega_{K0})$ for the XCDM parameterization and $(\Omega_{m0}, \alpha, \Omega_{K0})$ for the ϕ CDM model. Then using Eq. (3.1) we compute $\mathcal{L}_H(\boldsymbol{\theta})$ from $\mathcal{L}_H(\mathbf{p})$, and the two-dimensional confidence contours are obtained following the procedure discussed above.

¹²While performing the data analysis described in [39] we found that the two-dimensional contours obtained from integrating the likelihood function and those obtained by using the χ^2 prescription described here hardly differ. To save computational time we use the χ^2 prescription in this paper.

¹³In [39] we found that an augmented set of $H(z)$ measurements shows clear evidence for the cosmological deceleration-acceleration transition predicted to occur in cosmological models dominated by dark energy at the current epoch. [36] more clearly illustrate the presence of this transition in the data by binning and combining the $H(z)$ data.

¹⁴As discussed in [37], the constraint contours are sensitive to the H_0 prior used. The H_0 prior we use is obtained from a median statistics analysis [49] of 553 H_0 measurements [26], and has been stable now for more than a decade [24, 49]. Recent measurements of H_0 are consistent with this value [see e.g., 1, 30] although some suggest slightly larger or smaller values [see e.g., 42, 94, 98]. It may be significant that the value of H_0 we use does not demand the presence of dark radiation [20].

Table 1. Hubble Parameter Versus Redshift Data

z	$H(z)$ (km s ⁻¹ Mpc ⁻¹)	σ_H (km s ⁻¹ Mpc ⁻¹)	Reference ^a
0.090	69	12	1
0.170	83	8	1
0.179	75	4	4
0.199	75	5	4
0.240	79.69	2.65	2
0.270	77	14	1
0.352	83	14	4
0.400	95	17	1
0.430	86.45	3.68	2
0.480	97	62	3
0.593	104	13	4
0.680	92	8	4
0.781	105	12	4
0.875	125	17	4
0.880	90	40	3
0.900	117	23	1
1.037	154	20	4
1.300	168	17	1
1.430	177	18	1
1.530	140	14	1
1.750	202	40	1
2.300	224	8	5

^a (1) [92], (2) [45], (3) [95], (4) [67], (5) [18].

To tighten constraints on model parameters we also use a second data set, the [97] Union2.1 compilation of 580 SNIa distance modulus measurements at measured redshifts (covering the redshift range of 0.015 to 1.414) with corresponding one standard deviation uncertainties including systematic uncertainties. To constrain cosmological model parameters using this data the three-dimensional likelihood function $\mathcal{L}_{SN}(\mathbf{p})$ is defined by generalizing Eq. (26) of [37], marginalizing over a flat H_0 prior (for these SNIa data). Then using Eq. (3.1) we determine $\mathcal{L}_{SN}(\boldsymbol{\theta})$ from $\mathcal{L}_{SN}(\mathbf{p})$, and the two-dimensional confidence contours are obtained as discussed above.

The third set of data we consider are the 6 BAO peak length scale measurements (covering the redshift range of 0.1 to 0.75) with corresponding one standard deviation uncertainties, from [76], [13], and [15]. To constrain model parameters \mathbf{p} we compute the three-dimensional likelihood function $\mathcal{L}_{BAO}(\mathbf{p})$ by again marginalizing over a flat H_0 prior (for these BAO data), as discussed in Sec. 5 of [37]. Then using Eq. (3.1) we compute $\mathcal{L}_{BAO}(\boldsymbol{\theta})$ from $\mathcal{L}_{BAO}(\mathbf{p})$, and the two-dimensional confidence contours are obtained using the procedure discussed above.

Table 2. XCDM Parameterization Results

Data Set	Marginalization Range	Best-Fit Point	χ_{\min}^2	$\chi_{\min}^2/\text{d.o.f}$
$H(z)$	$\Omega_{K0} = 0^{\text{a}}$	$(\Omega_{m0}, \omega_X) = (0.27, -0.82)$	15.2	0.800
	$-0.7 \leq \Omega_{K0} \leq 0.7$	$(\Omega_{m0}, \omega_X) = (0.16, -1.35)$	17.8	0.937
	$-2 \leq \omega_X \leq 0$	$(\Omega_{m0}, \Omega_{K0}) = (0.16, 0.45)$	14.5	0.763
	$0 \leq \Omega_{m0} \leq 1$	$(\omega_X, \Omega_{K0}) = (-1.31, 0.44)$	20.4	1.074
SNIa	$\Omega_{K0} = 0^{\text{a}}$	$(\Omega_{m0}, \omega_X) = (0.29, -0.99)$	545	0.945
	$-0.7 \leq \Omega_{K0} \leq 0.7$	$(\Omega_{m0}, \omega_X) = (0.07, -0.57)$	546	0.946
	$-2 \leq \omega_X \leq 0$	$(\Omega_{m0}, \Omega_{K0}) = (0.28, 0.23)$	545	0.945
	$0 \leq \Omega_{m0} \leq 1$	$(\omega_X, \Omega_{K0}) = (-0.62, -0.46)$	549	0.951
BAO	$\Omega_{K0} = 0^{\text{a}}$	$(\Omega_{m0}, \omega_X) = (0.27, -1.21)$	5.50	1.833
	$-0.7 \leq \Omega_{K0} \leq 0.7$	$(\Omega_{m0}, \omega_X) = (0.27, -1.44)$	6.50	2.167
	$-2 \leq \omega_X \leq 0$	$(\Omega_{m0}, \Omega_{K0}) = (0.27, 0.09)$	4.90	1.633
	$0 \leq \Omega_{m0} \leq 1$	$(\omega_X, \Omega_{K0}) = (-1.44, -0.09)$	10.4	3.467
$H(z) + \text{SNIa}$	$\Omega_{K0} = 0^{\text{a}}$	$(\Omega_{m0}, \omega_X) = (0.27, -0.90)$	561	0.937
	$-0.7 \leq \Omega_{K0} \leq 0.7$	$(\Omega_{m0}, \omega_X) = (0.24, -0.97)$	562	0.938
	$-2 \leq \omega_X \leq 0$	$(\Omega_{m0}, \Omega_{K0}) = (0.18, 0.41)$	561	0.937
	$0 \leq \Omega_{m0} \leq 1$	$(\omega_X, \Omega_{K0}) = (-0.98, 0.15)$	566	0.945
$H(z) + \text{BAO}$	$\Omega_{K0} = 0^{\text{a}}$	$(\Omega_{m0}, \omega_X) = (0.29, -0.99)$	22.4	0.896
	$-0.7 \leq \Omega_{K0} \leq 0.7$	$(\Omega_{m0}, \omega_X) = (0.31, -0.79)$	24.2	0.968
	$-2 \leq \omega_X \leq 0$	$(\Omega_{m0}, \Omega_{K0}) = (0.31, -0.19)$	26.9	1.076
	$0 \leq \Omega_{m0} \leq 1$	$(\omega_X, \Omega_{K0}) = (-0.78, -0.19)$	27.5	1.100
SNIa + BAO	$\Omega_{K0} = 0^{\text{a}}$	$(\Omega_{m0}, \omega_X) = (0.30, -1.03)$	551	0.945
	$-0.7 \leq \Omega_{K0} \leq 0.7$	$(\Omega_{m0}, \omega_X) = (0.29, -0.77)$	553	0.949
	$-2 \leq \omega_X \leq 0$	$(\Omega_{m0}, \Omega_{K0}) = (0.31, 0.22)$	552	0.947
	$0 \leq \Omega_{m0} \leq 1$	$(\omega_X, \Omega_{K0}) = (-0.93, -0.10)$	556	0.954
$H(z) + \text{SNIa} + \text{BAO}$	$\Omega_{K0} = 0^{\text{a}}$	$(\Omega_{m0}, \omega_X) = (0.31, -1.02)$	566	0.936
	$-0.7 \leq \Omega_{K0} \leq 0.7$	$(\Omega_{m0}, \omega_X) = (0.30, -0.88)$	571	0.944
	$-2 \leq \omega_X \leq 0$	$(\Omega_{m0}, \Omega_{K0}) = (0.29, -0.15)$	582	0.962
	$0 \leq \Omega_{m0} \leq 1$	$(\omega_X, \Omega_{K0}) = (-0.90, -0.10)$	573	0.947

^a From [38].

Table 3. ϕ CDM Model Results

Data Set	Marginalization Range	Best-Fit Point	χ_{\min}^2	$\chi_{\min}^2/\text{d.o.f}$
$H(z)$	$\Omega_{K0} = 0^a$	$(\Omega_{m0}, \alpha) = (0.26, 0.70)$	15.2	0.800
	$-0.2 \leq \Omega_{K0} \leq 0.2$	$(\Omega_{m0}, \alpha) = (0.25, 1.12)$	17.8	0.937
	$0 \leq \alpha \leq 5$	$(\Omega_{m0}, \Omega_{K0}) = (0.21, 0.14)$	13.9	0.732
	$0 \leq \Omega_{m0} \leq 1$	$(\alpha, \Omega_{K0}) = (0.21, 0.19)$	20.4	1.074
SNIa	$\Omega_{K0} = 0^a$	$(\Omega_{m0}, \alpha) = (0.27, 0.20)$	545	0.945
	$-0.2 \leq \Omega_{K0} \leq 0.2$	$(\Omega_{m0}, \alpha) = (0.23, 0.64)$	548	0.948
	$0 \leq \alpha \leq 5$	$(\Omega_{m0}, \Omega_{K0}) = (0.23, -0.15)$	547	0.948
	$0 \leq \Omega_{m0} \leq 1$	$(\alpha, \Omega_{K0}) = (0.08, -0.03)$	550	0.953
BAO	$\Omega_{K0} = 0^a$	$(\Omega_{m0}, \alpha) = (0.30, 0.00)$	5.9	1.967
	$-0.2 \leq \Omega_{K0} \leq 0.2$	$(\Omega_{m0}, \alpha) = (0.30, 0.01)$	8.30	2.767
	$0 \leq \alpha \leq 5$	$(\Omega_{m0}, \Omega_{K0}) = (0.32, -0.20)$	5.50	1.833
	$0 \leq \Omega_{m0} \leq 1$	$(\alpha, \Omega_{K0}) = (0.08, -0.15)$	10.6	3.533
$H(z) + \text{SNIa}$	$\Omega_{K0} = 0^a$	$(\Omega_{m0}, \alpha) = (0.26, 0.35)$	561	0.937
	$-0.2 \leq \Omega_{K0} \leq 0.2$	$(\Omega_{m0}, \alpha) = (0.26, 0.31)$	564	0.942
	$0 \leq \alpha \leq 5$	$(\Omega_{m0}, \Omega_{K0}) = (0.25, 0.11)$	562	0.938
	$0 \leq \Omega_{m0} \leq 1$	$(\alpha, \Omega_{K0}) = (0.09, 0.08)$	567	0.947
$H(z) + \text{BAO}$	$\Omega_{K0} = 0^a$	$(\Omega_{m0}, \alpha) = (0.29, 0.00)$	22.4	0.896
	$-0.2 \leq \Omega_{K0} \leq 0.2$	$(\Omega_{m0}, \alpha) = (0.30, 0.34)$	25.2	1.008
	$0 \leq \alpha \leq 5$	$(\Omega_{m0}, \Omega_{K0}) = (0.31, -0.20)$	21.9	0.876
	$0 \leq \Omega_{m0} \leq 1$	$(\alpha, \Omega_{K0}) = (0.77, -0.20)$	27.5	1.100
SNIa + BAO	$\Omega_{K0} = 0^a$	$(\Omega_{m0}, \alpha) = (0.30, 0.00)$	551	0.945
	$-0.2 \leq \Omega_{K0} \leq 0.2$	$(\Omega_{m0}, \alpha) = (0.30, 0.08)$	554	0.950
	$0 \leq \alpha \leq 5$	$(\Omega_{m0}, \Omega_{K0}) = (0.30, -0.05)$	553	0.949
	$0 \leq \Omega_{m0} \leq 1$	$(\alpha, \Omega_{K0}) = (0.02, -0.03)$	557	0.955
$H(z) + \text{SNIa} + \text{BAO}$	$\Omega_{K0} = 0^a$	$(\Omega_{m0}, \alpha) = (0.29, 0.00)$	567	0.937
	$-0.2 \leq \Omega_{K0} \leq 0.2$	$(\Omega_{m0}, \alpha) = (0.30, 0.46)$	571	0.944
	$0 \leq \alpha \leq 5$	$(\Omega_{m0}, \Omega_{K0}) = (0.30, -0.05)$	569	0.940
	$0 \leq \Omega_{m0} \leq 1$	$(\alpha, \Omega_{K0}) = (0.01, 0.00)$	573	0.947

^a From [38].

Figures 1 and 2 show the constraints on parameters of the XCDM parameterization and the ϕ CDM model from the $H(z)$ (top row), SNIa (middle row), and BAO (bottom row) measurements. In these figures the panels in the first, second, and third columns show the two-dimensional probability density constraint contours (solid lines) from $\mathcal{L}(\Omega_{m0}, \omega_X)[\mathcal{L}(\Omega_{m0}, \alpha)]$, $\mathcal{L}(\Omega_{m0}, \Omega_{K0})$, and $\mathcal{L}(\omega_X, \Omega_{K0})[\mathcal{L}(\alpha, \Omega_{K0})]$ for the XCDM parameterization [the ϕ CDM model]. The dot-dashed contours in the panels of the first columns of Figs. (1) and (2) are 1σ , 2σ , and 3σ confidence contours corresponding to spatially-flat models, reproduced from [38]. Tables 2 and 3 list best-fit points and χ_{\min}^2 values.

Comparing the solid contours to the dot-dashed contours in the panels in the first columns of Figs. 1 and 2, we see that the addition of space curvature as a third free parameter results in a fairly significant broadening of the constraint contours, as might have been anticipated. For the XCDM parameterization (first column of Fig. 1), since the data constrain ω_X reasonably well in the spatially-flat case, the inclusion of space curvature as

a free parameter significantly weakens the bounds on ω_X . For the ϕ CDM model (first column of Fig. 2) the data do not constrain α (the corresponding parameter that governs the time-variability of dark energy in this case) as tightly in the spatially-flat case, so inclusion of space curvature appears to have a relatively less significant effect (this is probably also a consequence of the significantly smaller Ω_{K0} range considered, $-0.2 \leq \Omega_{K0} \leq 0.2$, for computational tractability). This interplay between space curvature and the parameter that governs the time-variability of dark energy is also evident in the second and third columns of panels of Figs. 1 and 2. Clearly, for the single data sets, including space curvature in the analysis significantly weakens the support for a constant cosmological constant Λ , while allowing dark energy density to be dynamical significantly weakens support for a spatially-flat model. The reason for this is that the space curvature energy density redshifts in a way that is closer to the behavior of the dark energy density than does the non-relativistic matter density.

These results show very clearly that when spatial curvature is a free parameter a single data set cannot significantly constrain cosmological parameters of the dynamical dark energy models considered here. To tighten constraints on cosmological parameters, we next consider combinations of data sets.

3.2 Constraints from combinations of data sets

Figures 3 and 4 show constraints on the parameters of the XCDM parameterization and the ϕ CDM model from the $H(z)$ +SNIa (top row), $H(z)$ +BAO (middle row), and SNIa+BAO (bottom row) measurements. In these figures the panels in the first, second, and third columns show the two-dimensional probability density constraint contours (solid lines) from $\mathcal{L}(\Omega_{m0}, \omega_X)[\mathcal{L}(\Omega_{m0}, \alpha)]$, $\mathcal{L}(\Omega_{m0}, \Omega_{K0})$, and $\mathcal{L}(\omega_X, \Omega_{K0})[\mathcal{L}(\alpha, \Omega_{K0})]$ for the XCDM parameterization [the ϕ CDM model]. The dot-dashed contours in the panels of the first columns of Figs. 3 and 4 are 1σ , 2σ , and 3σ confidence contours corresponding to spatially-flat models, reproduced from [38]. Tables 2 and 3 list best-fit points and χ^2_{\min} values.

Comparing the solid contours of Figs. 3 and 4 to those derived from the single data sets in Figs. 1 and 2, we see that combinations of pairs of data sets result in a significant tightening of constraints, especially on Ω_{m0} , and less so on Ω_{K0} , ω_X , and α .

Comparing the solid contours to the dot-dashed contours in the panels in the first columns of Figs. 3 and 4 we see that the addition of space curvature as a third free parameter results in a fairly significant broadening of the constraint contours, even when using two data sets at a time, particularly in the direction along the parameter that governs the time evolution of the dark energy density (ω_X for the XCDM parameterization and α for the ϕ CDM model). Again, when space curvature is included as a free parameter the constraint contours broaden more significantly for the XCDM parameterization than for the ϕ CDM model: compare the solid and dot-dashed contours in the first columns of Figs. 3 and 4 (this is probably partially a consequence of the smaller range of space curvature, $-0.2 \leq \Omega_{K0} \leq 0.2$, considered for computational tractability in the ϕ CDM case).

Encouraged by the tightening of the constraint contours when two data sets are analyzed together, we now discuss the result of a joint analysis of the $H(z)$, SNIa, and BAO data. Figures 5 and 6 show constraints on the parameters of the XCDM parameterization and the ϕ CDM model from the $H(z)$ +SNIa+BAO measurements. In these figures the top left panel, top right panel, and the bottom panel show the two-dimensional probability density constraint contours (solid lines) from $\mathcal{L}(\Omega_{m0}, \omega_X)[\mathcal{L}(\Omega_{m0}, \alpha)]$, $\mathcal{L}(\Omega_{m0}, \Omega_{K0})$, and $\mathcal{L}(\omega_X, \Omega_{K0})[\mathcal{L}(\alpha, \Omega_{K0})]$ for the XCDM parameterization [the ϕ CDM model]. The dot-dashed contours in the left top panels of Figs. (5) and (6) are 1σ , 2σ , and 3σ confidence contours

corresponding to spatially-flat models, reproduced from [38]. Tables 2 and 3 list best-fit points and χ_{\min}^2 values.

Comparing the solid contours of Figs. 5 and 6 to those derived from the data set pairs of Figs. 3 and 4, we see that the joint analysis of all three data sets results in a significant tightening of constraints.

Comparing the solid contours to the dot-dashed contours in the left top panels in Figs. 5 and 6 we see that the addition of space curvature as a third free parameter results in a significant broadening of the constraint contours, but this time less than when only two data sets were used in Figs. 3 and 4. The broadening is more significant in the direction along the parameter that governs the time evolution of the dark energy density (ω_X for the XCDM parameterization and α for the ϕ CDM model).

We also computed the 1σ and 2σ bounds on model parameters that follow from the joint analysis of $H(z)$, SNIa, and BAO measurements. Tables 4 and 5 list these bounds on individual cosmological parameters, determined from their one-dimensional posterior probability distribution functions (which we obtained by marginalizing the three-dimensional likelihood over the other two cosmological parameters). The numerical values listed in these tables confirm the results described in the discussion above of Figs. 5 and 6.

Table 4. XCDM Parametrization Results From $H(z)$ +SNIa+BAO Data

Marginalization Range	1σ intervals	2σ intervals
$\Omega_{K0} = 0^a$	$0.29 \leq \Omega_{m0} \leq 0.31$	$0.27 \leq \Omega_{m0} \leq 0.32$
	$-1.01 \leq \omega_X \leq -0.83$	$-1.03 \leq \omega_X \leq -0.77$
$-0.7 \leq \Omega_{K0} \leq -0.7$	$0.27 \leq \Omega_{m0} \leq 0.32$	$0.25 \leq \Omega_{m0} \leq 0.34$
	$-1.03 \leq \omega_X \leq -0.77$	$-1.25 \leq \omega_X \leq -0.69$
$-2 \leq \omega_X \leq 0$	$0.27 \leq \Omega_{m0} \leq 0.32$	$0.25 \leq \Omega_{m0} \leq 0.34$
	$-0.21 \leq \Omega_{K0} \leq 0.10$	$-0.39 \leq \Omega_{K0} \leq 0.22$
$0 \leq \Omega_{m0} \leq 1$	$-1.03 \leq \omega_X \leq -0.77$	$-1.30 \leq \omega_X \leq -0.69$
	$-0.21 \leq \Omega_{K0} \leq 0.10$	$-0.39 \leq \Omega_{K0} \leq 0.22$

^a From [38].

Table 5. ϕ CDM Model Results From $H(z)$ +SNIa+BAO Data

Marginalization Range	1σ intervals	2σ intervals
$\Omega_{K0} = 0^a$	$0.27 \leq \Omega_{m0} \leq 0.29$	$0.25 \leq \Omega_{m0} \leq 0.30$
	$\alpha \leq 0.31$	$\alpha \leq 0.56$
$-0.2 \leq \Omega_{K0} \leq -0.2$	$0.28 \leq \Omega_{m0} \leq 0.32$	$0.26 \leq \Omega_{m0} \leq 0.34$
	$\alpha \leq 1.03$	$\alpha \leq 1.64$
$0 \leq \alpha \leq 5^b$	$0.28 \leq \Omega_{m0} \leq 0.31$	$0.26 \leq \Omega_{m0} \leq 0.33$
	$-0.2 \leq \Omega_{K0} \leq 0.09$	$-0.2 \leq \Omega_{K0} \leq 0.12$
$0 \leq \Omega_{m0} \leq 1^b$	$\alpha \leq 1.03$	$\alpha \leq 1.64$
	$-0.2 \leq \Omega_{K0} \leq 0.09$	$-0.2 \leq \Omega_{K0} \leq 0.12$

^a From [38].

^b The lower limit on Ω_{K0} is determined by the lower limit of the $\Omega_{K0} \geq -0.2$ prior assumed for the case of ϕ CDM, not from the observational data. However, we strongly suspect that this limit will not change greatly with an increase of the integration limit for the data used here.

Of some interest are the bounds on the curvature density parameter Ω_{K0} . Perhaps the most useful summary is the 1σ limit $|\Omega_{K0}| \lesssim 0.15$ derived by symmetrizing about $\Omega_{K0} = 0$ the 1σ range from the central columns of Table 4 and 5. Note that the possible 2σ range of Ω_{K0} is significantly smaller for ϕ CDM than for XCDM (compare the relevant entries in the last columns of Table 4 and 5). This is almost certainly a consequence of the smaller range of Ω_{K0} , $-0.2 \leq \Omega_{K0} \leq 0.2$, we have used in the ϕ CDM computation; the 2σ XCDM bound $|\Omega_{K0}| \lesssim 0.3$ is the more reliable one.

4 Conclusion

A joint analysis of $H(z)$, SNIa, and BAO data using the XCDM parametrization and the ϕ CDM model of time evolving dark energy density in a non-flat geometry leads to the conclusion that more, and more precise, data are required to tightly pin down the spatial curvature of the Universe in dynamical dark energy models. These data require $|\Omega_{K0}| \lesssim 0.15$ at 1σ confidence. It would be of interest to determine the constraints on space curvature in the non-flat ϕ CDM model from CMB anisotropy measurements. Such an analysis, possibly in combination with that of other data of the kind considered here, and extended over a wider range of Ω_{K0} than we have considered, could go a long way towards establishing whether space curvature contributes significantly to the current cosmological energy budget.

Acknowledgments

We thank Mikhail Makouski, Anatoly Pavlov, and Shawn Westmoreland for useful discussions and helpful advice. We thank Daniel Nelson for allowing us to use his computer for some of the computations. This work was supported in part by DOE grant DEFG03-99EP41093 and NSF grant AST-1109275.

References

- [1] Ade, P. A. R., et al. 2013, arXiv:1303.5076 [astro-ph.CO]
- [2] Allen, S. W., et al. 2008, MNRAS, 383, 879
- [3] Appleby, S. A., & Linder, E., 2013, Phys. Rev. D, 87, 023532
- [4] Arabsalmani, M., Sahni, V., & Saini, T., D., 2013, Phys. Rev. D, 87, 083001
- [5] Aurich, R., & Steiner, F. 2002, MNRAS, 334, 735
- [6] Aurich, R., & Steiner, F. 2003, Phys. Rev. D, 67, 123511
- [7] Aurich, R., & Steiner, F. 2004, Int. J. Mod. Phys. D 13, 123
- [8] Ayaita, Y., Weber, M., & Wetterich, C., 2012, Phys. Rev. D, 87, 043519
- [9] Basse, T., et al. 2012, arXiv:1205.0548 [astro-ph.CO]
- [10] Batista, R., C., & Pace, F., 2013, arXiv:1303.0414 [astro-ph.CO]
- [11] Benaoum, H. B., 2012, arXiv:1211.3518 [gr-qc]
- [12] Bezrukov, F., et al. 2013, Phys. Rev. D, 87, 096001
- [13] Beutler, F., et al. 2011, MNRAS, 416, 3077
- [14] Biesiada, M., Piórkowska, A., & Malec, B. 2010, MNRAS, 406, 1055
- [15] Blake, C., et al. 2011, MNRAS, 418, 1707

- [16] Bonamente, M., et al. 2006, ApJ, 647, 25
- [17] Bucher, M., Goldhaber, A. S., & Turok, N., 1995, Phys. Rev. D, 52, 3314
- [18] Busca, N. G., et al. 2012, arXiv:1211.2616 [astro-ph]
- [19] Busti, V. C., Santos, R. C., & Lima, J. A. S. 2012, Phys. Rev. D, 85, 103503
- [20] Calabrese, E., et al. 2012, Phys. Rev. D, 86, 043520
- [21] Campbell, H., et al. 2013, ApJ, 763, 88
- [22] Capozziello, S., & De Laurentis, M. 2011, Phys. Rept., 509, 167
- [23] Chae, K.-H., et al. 2004, ApJ, 607, L71
- [24] Chen, G., Gott, J. R., & Ratra, B. 2003, PASP, 115, 1269
- [25] Chen, G., & Ratra, B. 2003, PASP, 115, 1143
- [26] Chen, G., & Ratra, B. 2011a, PASP, 123, 1127
- [27] Chen, Y., & Ratra, B. 2011b, Phys. Lett. B, 703, 406
- [28] Chen, Y., & Ratra, B. 2012, A&A, 543, A104
- [29] Chen, Z.-Q., & Guo, D. H., 2012, Int. J. Theor. Phys., 51, 3856
- [30] Colless, M., Beutler, F., & Blake, C. 2012, arXiv:1211.2570 [astro-ph.CO]
- [31] Crooks, J. L., et al. 2003, Astropart. Phys., 20, 361
- [32] Davis, T. M., et al. 2007, ApJ, 666, 716
- [33] De Boni, C., 2013, arXiv:1302.2364 [astro-ph.CO]
- [34] Devi, N. C., Choudhury, T. R., & Sen, A. A. 2011, arXiv:1112.0728 [astro-ph.CO]
- [35] Dossett, J. N., & Ishak, M. 2012, Phys. Rev. D, 86, 103008
- [36] Farooq, O., Crandall, S., & Ratra, B. 2013b, arXiv:1305.1957 [astro-ph.CO]
- [37] Farooq, O., Mania, D., & Ratra, B. 2013a, ApJ, 764, 138
- [38] Farooq, O., & Ratra, B. 2013a, Phys. Lett. B, 723, 1
- [39] Farooq, O., & Ratra, B. 2013b, ApJ, 766, L7
- [40] Ferreira, P. C., Carvalho, J., C., & Alcaniz, J., S., 2013, Phys. Rev. D, 87, 087301
- [41] Fischler, W., Ratra, B., & Susskind, L., 1985, Nucl. Phys. B, 259, 730
- [42] Freedman, W. L., et al. 2012, ApJ, 758, 24
- [43] Ganga, K., et al. 1997, ApJ, 484, 7
- [44] Garcia-Salcedo, R., Gonzalez, T., & Quiros, I. 2012, arXiv:1211.2738 [gr-qc]
- [45] Gaztañaga, E., Cabré, A., & Hui, L. 2009, MNRAS, 399,1663
- [46] Gong, Y., Wu, Q., & Wang, A. 2008, ApJ, 681, 27
- [47] Górski, K. M., et al. 1998, ApJS, 114, 1
- [48] Gott, J. R., 1982, Nature, 295, 304
- [49] Gott, J. R., et al. 2001, ApJ, 549, 1
- [50] Guerra, E. J., Daly, R. A., & Wan, L. 2000, ApJ, 544, 659
- [51] Gumjudpai, B., & Thepsuriya, K. 2012, ArSS, 342, 537
- [52] Ichikawa, K., et al. 2006, J. Cosmology Astropart. Phys., 0612, 005
- [53] Ichikawa, K., & Takahashi, T. 2006, Phys. Rev. D, 73, 083526

- [54] Ichikawa, K., & Takahashi, T. 2007, *J. Cosmology Astropart. Phys.*, 0702, 001
- [55] Ichikawa, K., & Takahashi, T. 2008, *J. Cosmology Astropart. Phys.*, 0804, 027
- [56] Jassal, H. K., Bagla, J. S., & Padmanabhan, T. 2010, *MNRAS*, 405, 2639
- [57] Kamionkowski, M., et al. 1994, *ApJ*, 434, L1
- [58] Landry, D., et al. 2012, arXiv:1211.4626 [astro-ph.CO]
- [59] Lee, S., & Ng, K.-W. 2007, *Phys. Rev. D*, 76, 043518
- [60] Liao, K., & Zhu, Z.-H. 2013, *Phys. Lett. B*, 718, 1155
- [61] Li, M., et al. 2012, arXiv:1209.0992 [astro-ph.CO]
- [62] Liu, W., Ouyang, J., & Yang, H.-X. 2012, arXiv:1211.0219 [astro-ph.CO]
- [63] Lu, J., et al. 2011, *Eur. Phys. J. C*, 71, 1800
- [64] Lyth, D. H. & Woszczyna, A. 1995, *Phys. Rev. D*, 52, 3338
- [65] Mania, D., & Ratra, B. 2012, *Phys. Lett. B*, 715, 9
- [66] Mehta, K. T., et al. 2012, arXiv:1202.0092 [astro-ph.CO]
- [67] Moresco, M., et al. 2012, *J. Cosmology Astropart. Phys.*, 1208, 006
- [68] Mortonson, M. J. 2009, *Phys. Rev. D*, 80, 123504
- [69] Mortonson, M. J., Hu, W., & Huterer, D. 2011, *Phys. Rev. D*, 83, 023015
- [70] Pan, Y., et al., 2013, *Phys. Lett. B*, 718, 699
- [71] Pavlov, A., Samushia, L., & Ratra, B. 2012, *ApJ*, 760, 19
- [72] Pavlov, A., et al. 2013, arXiv:1307.7399 [astro-ph.CO]
- [73] Peebles, P. J. E. 1984, *ApJ*, 284, 439
- [74] Peebles, P. J. E., & Ratra, B. 1988, *ApJ*, 325, L17
- [75] Peebles, P. J. E., & Ratra, B. 2003, *Rev. Mod. Phys.*, 75, 559
- [76] Percival, W. J., et al. 2010, *MNRAS*, 401, 2148
- [77] Plionis, M., et al. 2010, *AIP Conf. Proc.* 1241, 267
- [78] Plionis, M., et al. 2011, *MNRAS*, 416, 2981
- [79] Podariu, S., Nugent, P., & Ratra, B. 2001, *ApJ*, 553, 39
- [80] Podariu, S., et al. 2001, *ApJ*, 559, 9
- [81] Podariu, S., & Ratra, B. 2000, *ApJ*, 532, 109
- [82] Ratra, B. 1991, *Phys. Rev. D*, 43, 3802
- [83] Ratra, B. 1992, *Phys. Rev. D*, 45, 1913
- [84] Ratra, B., & Peebles, P. J. E. 1988, *Phys. Rev. D*, 37, 3406
- [85] Ratra, B., & Peebles, P. J. E. 1994, *ApJ*, 432, L5
- [86] Ratra, B., & Peebles, P. J. E. 1995, *Phys. Rev. D*, 52, 1837
- [87] Salzano, V., et al. 2012, arXiv:1211.1012 [astro-ph.CO]
- [88] Samushia, L., & Ratra, B. 2008, *ApJ*, 680, L1
- [89] Samushia, L., & Ratra, B. 2010, *ApJ*, 714, 1347
- [90] Samushia, L., et al. 2011, *MNRAS*, 410, 1993
- [91] Sartoris, B., et al. 2012, *MNRAS*, 423, 2503

- [92] Simon, J., Verde, L., & Jimenez, R. 2005, *Phys. Rev. D*, 71, 123001
- [93] Solà, J. 2013, arXiv:1306.1527 [gr-qc]
- [94] Sorce, J. G., Tully, R. B., & Courtois, H. M. 2012, *ApJ*, 758, L12
- [95] Stern, D., et al. 2010, *JCAP* 1002 (2010) 008
- [96] Suyu, S. H., et al. 2013, *ApJ*, 766, 70
- [97] Suzuki, N., et al. 2012, *ApJ*, 746, 85
- [98] Tammann, G. A., & Reindl, B. 2012, arXiv:1211.4655 [astro-ph.CO]
- [99] Thepsuriya, K., & Gumjudpai, B. 2009, arXiv:0904.2743 [astro-ph.CO]
- [100] Tong, M., & Noh, H. 2011, *Eur. Phys. J. C*, 71, 1586
- [101] Trodden, M. 2012, arXiv:1212.6399 [astro-ph.CO]
- [102] Tsujikawa, S. 2013, arXiv:1304.1961 [gr-qc]
- [103] Virey, J-M., et al. 2008, *J. Cosmology Astropart. Phys.*, 0812, 008
- [104] Wang, F. Y., & Dai, J. G. 2011, *A&A*, 536, A96
- [105] Wang, X., et al. 2012, *J. Cosmology Astropart. Phys.*, 1211, 018
- [106] Wang, Y. 2012, *MNRAS*, 423, 3631
- [107] Wang, Y., & Mukherjee, P. 2007, *Phys. Rev. D*, 76, 103533
- [108] Weinberg, D. H., et al. 2013, arXiv:1306.0913 [astro-ph.CO]
- [109] Wilson, K. M., Chen, G., & Ratra, B. 2006, *Mod. Phys. Lett. A*, 21, 2197
- [110] Wright, E. L., 2006, arXiv:0603750 [astro-ph.CO]
- [111] Yamamoto, K., Sasaki, M., & Tanaka, T. 1995, *ApJ*, 455, 412
- [112] Zhang, C., et al. 2012, arXiv:1207.4541 [astro-ph.CO]
- [113] Zhao, G-B., et al. 2007, *Phys. Lett. B*, 648, 8

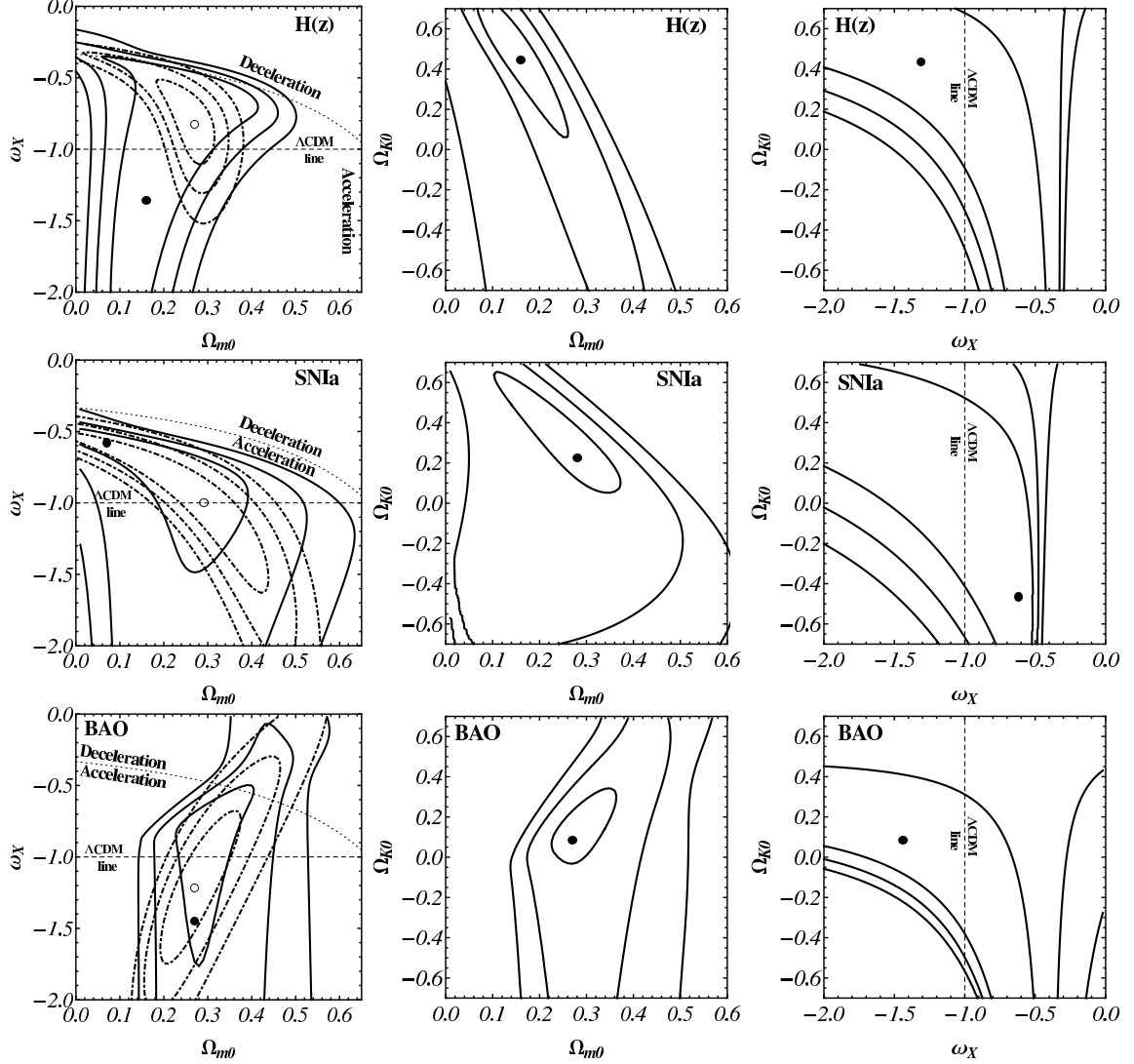


Figure 1. 1σ , 2σ , and 3σ constraint contours (solid lines) for parameters of the non-flat XCDM dark energy parameterization from $H(z)$ (first row), SNIa (second row), and BAO (third row) measurements; filled circles show best-fit points. The dot-dashed lines in the first column panels are 1σ , 2σ , and 3σ constraint contours derived by [38] using the spatially-flat XCDM parameterization (open circles show best-fit points); here dotted lines distinguish between accelerating and decelerating models (at zero space curvature) and dashed lines (here and in the third column) correspond to the Λ CDM model. First, second, and third columns correspond to marginalizing over Ω_{K0} , ω_X , and Ω_{m0} respectively.

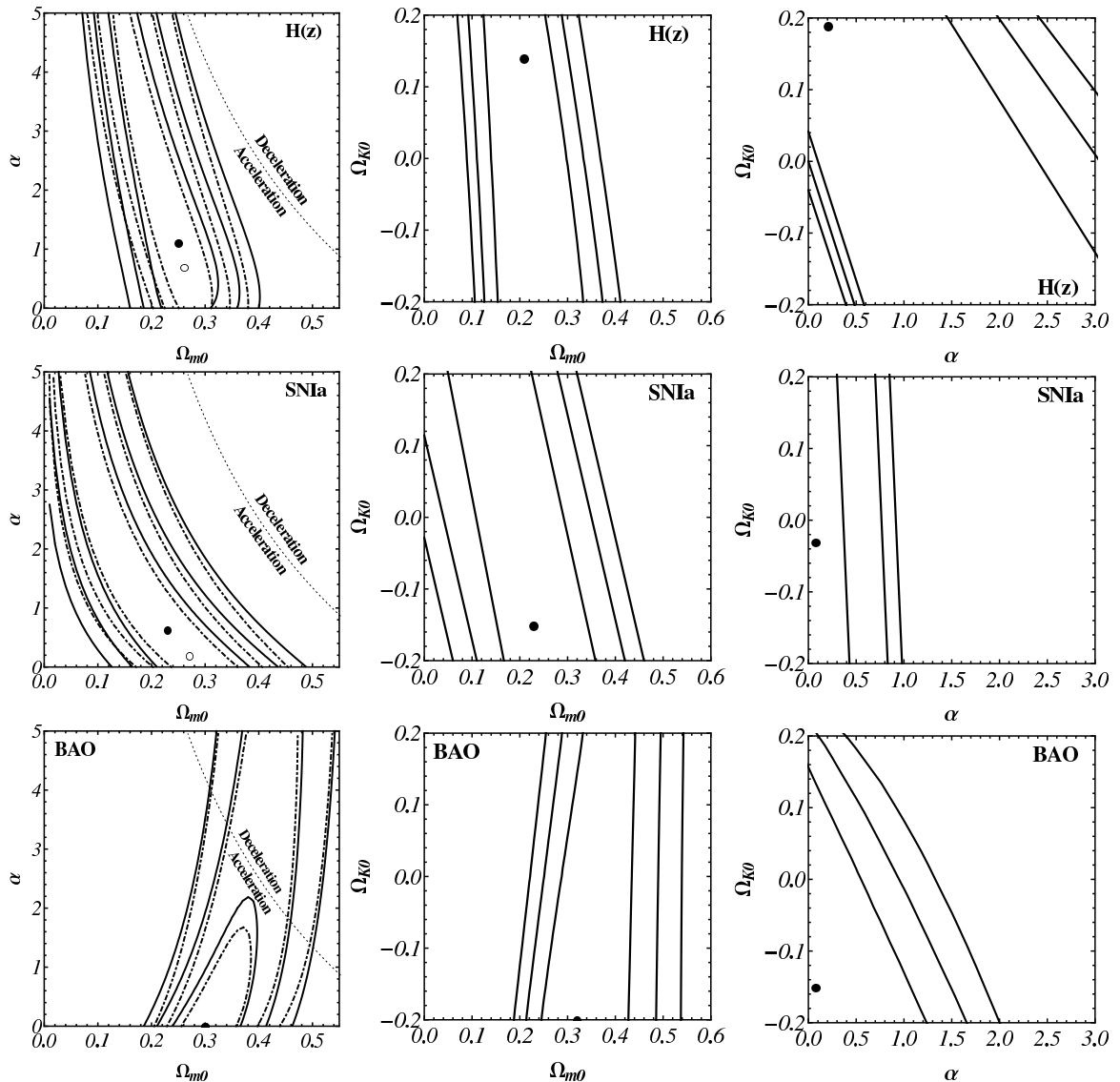


Figure 2. 1σ , 2σ , and 3σ constraint contours (solid lines) for parameters of the non-flat ϕ CDM dark energy model from $H(z)$ (first row), SNIa (second row), and BAO (third row) measurements; filled circles show best-fit points. The dot-dashed lines in the first column panels are 1σ , 2σ , and 3σ constraint contours derived by [38] using the spatially-flat ϕ CDM model (open circles show best-fit points); here dotted lines distinguish between accelerating and decelerating models (at zero space curvature) and the $\alpha = 0$ axes (here and in the third column) correspond to the Λ CDM model. First, second, and third columns correspond to marginalizing over Ω_{K0} , α , and Ω_{m0} respectively. We note that the $\Omega_{K0} = 0$ constraints and the marginalized Ω_{K0} constraints differ by only a small amount due to the prior range of Ω_{K0} used here.

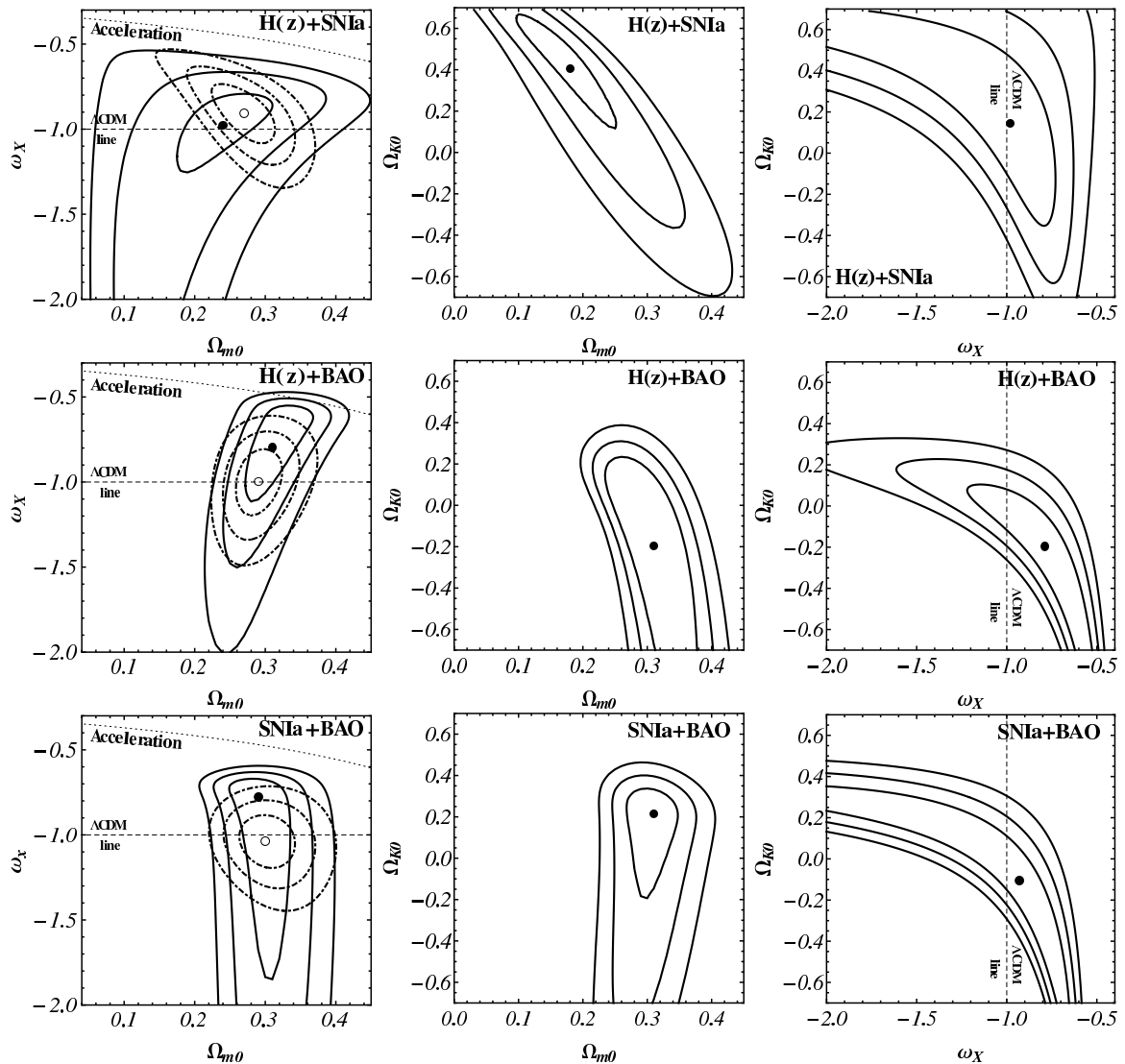


Figure 3. 1σ , 2σ , and 3σ constraint contours (solid lines) for parameters of the non-flat XCDM dark energy parameterization from $H(z)$ +SNIa (first row), $H(z)$ +BAO (second row), and SNIa+BAO (third row) measurements; filled circles show best-fit points. The dot-dashed lines in the first column panels are 1σ , 2σ , and 3σ constraint contours derived by [38] using the spatially-flat XCDM dark energy parameterization (open circles show best-fit points); here dotted lines distinguish between accelerating and decelerating models (at zero space curvature) and dashed lines (here and in the third column) correspond to the Λ CDM model. First, second, and third columns correspond to marginalizing over Ω_{K0} , ω_X , and Ω_{m0} respectively.

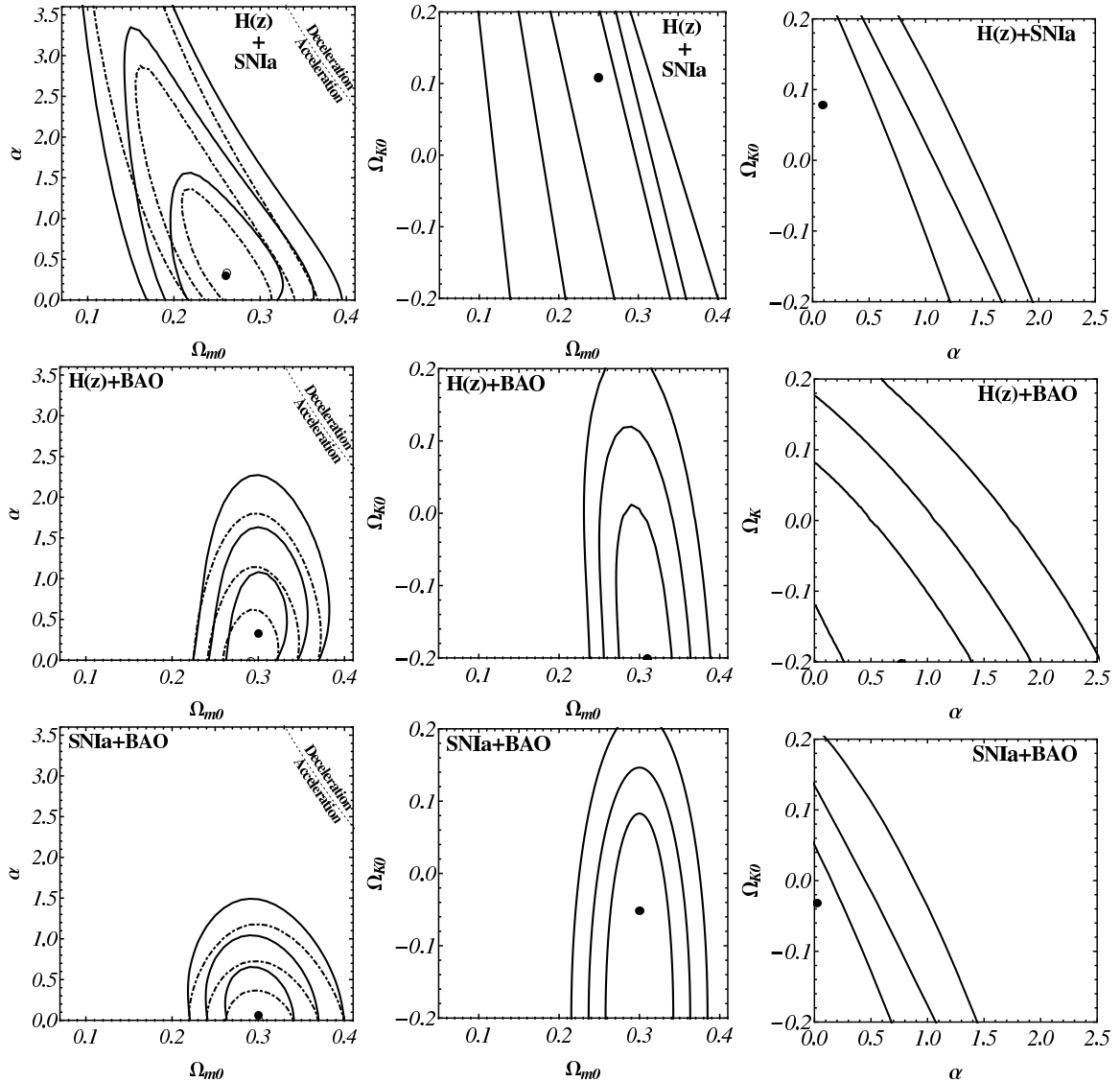


Figure 4. 1σ , 2σ , and 3σ constraint contour (solid lines) for parameters of the non-flat ϕ CDM dark energy model from $H(z)$ +SNIa (first row), $H(z)$ +BAO (second row), and BAO+SNIa (third row) measurements; filled circles show best-fit points. The dot-dashed lines in the first column panels are 1σ , 2σ , and 3σ constraint contours derived by [38] using the spatially-flat ϕ CDM model (open circles show best-fit points); here dotted lines distinguish between accelerating and decelerating models (at zero space curvature) and the $\alpha = 0$ axes (here and in the third column) correspond to the Λ CDM model. First, second, and third columns correspond to marginalizing over Ω_{K0} , α , and Ω_{m0} respectively. We note that the $\Omega_{K0} = 0$ constraints and the marginalized Ω_{K0} constraints differ by only a small amount due to the prior range of Ω_{K0} used here.

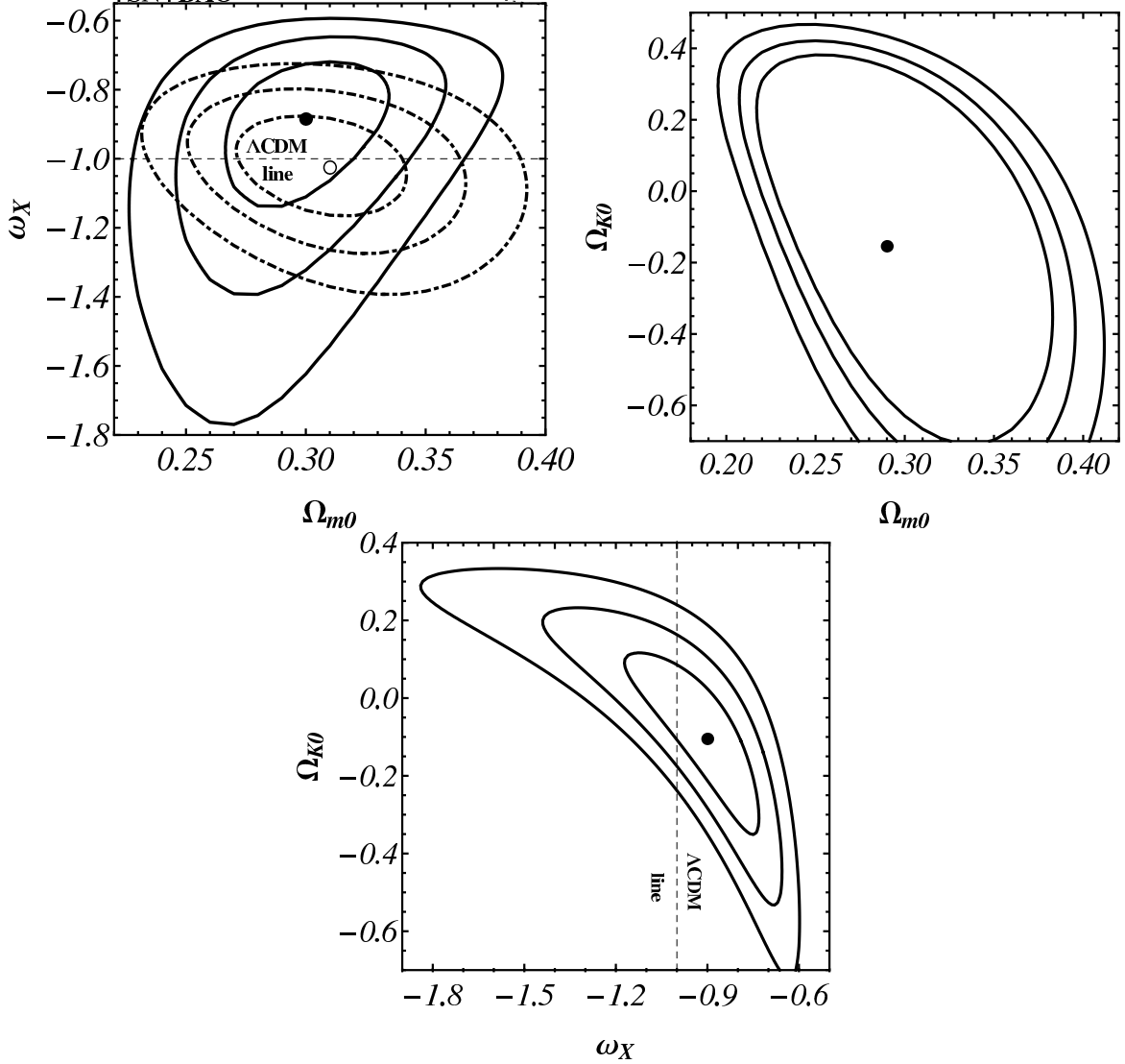


Figure 5. 1σ , 2σ , and 3σ constraint contours (solid lines) for parameters of the non-flat XCDM dark energy parameterization from $H(z)$ +SNIa+BAO measurements; filled circles show best-fit points. The dot-dashed lines in the top left panel are 1σ , 2σ , and 3σ constraint contours derived by [38] using the spatially-flat XCDM parameterization (open circle shows best-fit point); here dashed lines (in the top left and bottom panels) correspond to the Λ CDM model. Top left, top right, and bottom panel correspond to marginalizing over Ω_{K0} , ω_X , and Ω_{m0} respectively.

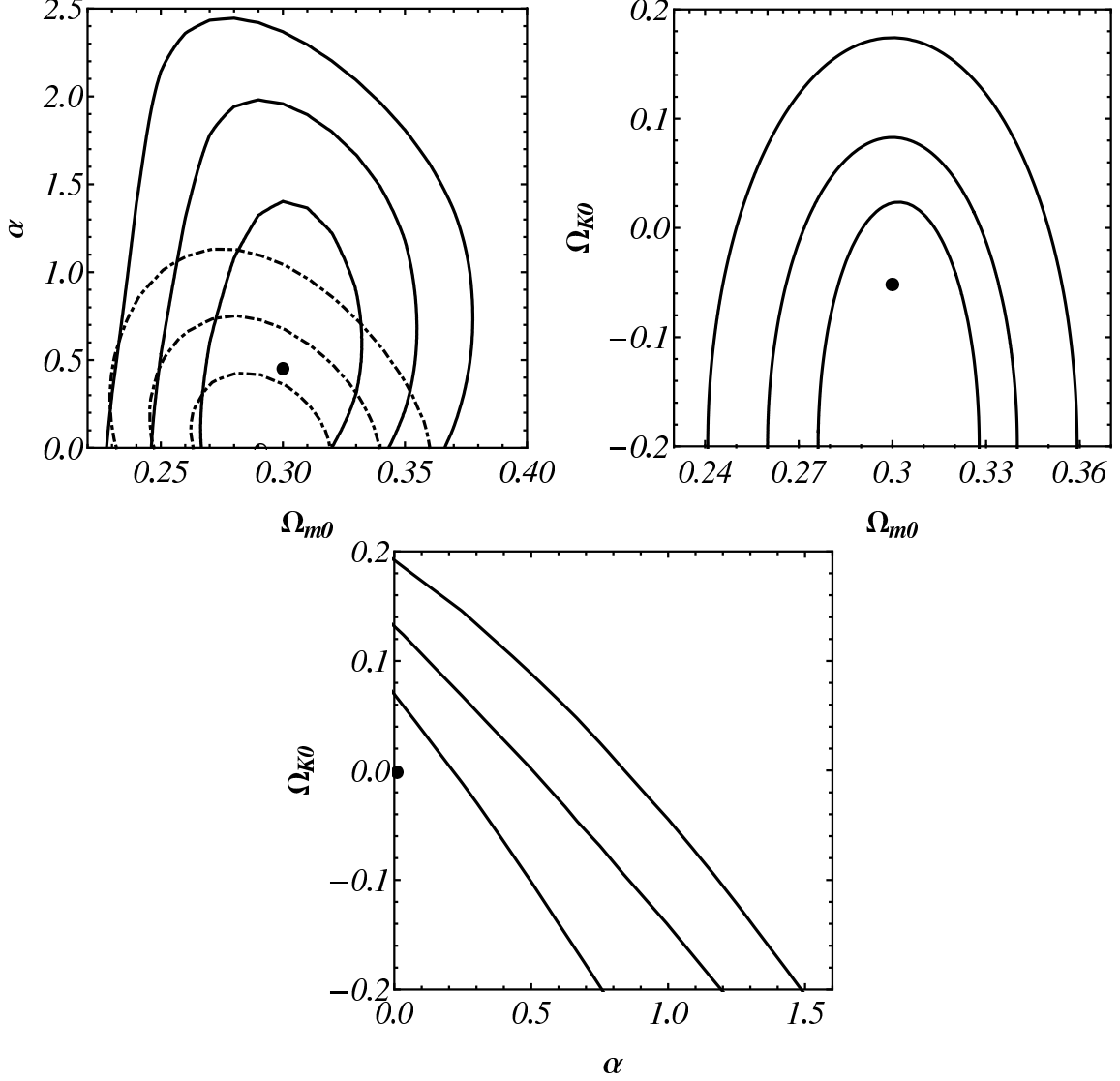


Figure 6. 1 σ , 2 σ , and 3 σ constraint contours (solid lines) for parameters of the non-flat ϕ CDM dark energy model from $H(z)$ +SNIa+BAO measurements; filled circles show best-fit points. The dot-dashed lines are 1 σ , 2 σ , and 3 σ constraint contours derived by [38] using the spatially-flat ϕ CDM model (open circle shows best-fit point); here the $\alpha = 0$ axes in the top left and bottom panels correspond to the Λ CDM model. Top left, top right, and bottom panel correspond to marginalizing over Ω_{K0} , α , and Ω_{m0} respectively.